

# Design Study of the Injection and Extraction Systems for the RIKEN Superconducting Ring Cyclotron

H. OKUNO, T. TOMINAKA, S. FUJISHIMA, A. GOTO, AND Y. YANO

*The Institute of Physical and Chemical Research (RIKEN), Wako, Saitama, 351-0198, Japan*

Superconducting magnets for the injection system of the six-sector superconducting ring cyclotron (SRC), which has been proposed at RIKEN as one of post accelerators of the existing room-temperature ring cyclotron, are designed. Characteristics and structure design of the magnets are given. A design study of injection and extraction systems in a four-cavity configuration in the SRC is also briefly described.

## 1 Introduction

In the RI beam factory project[1], an intermediate-stage ring cyclotron and a six-sector superconducting ring cyclotron (IRC and SRC)[2] are designed to boost the energy of the ion beams available from the existing RIKEN Ring Cyclotron (RRC). The output energies of the SRC are 400 MeV/u for light ions such as carbon and are 150 MeV/u for heavy ions such as uranium. The injection energies ( $E_{inj}$ ), required to obtain the designed output energies ( $E_{ext}$ ), for three kinds of ion beams, are shown in Table 1. Figure 1 shows an example of the trajectories of injected beams in the SRC. The beams are injected through one of the magnetic valleys into the central region of the SRC, which are then radially guided to their first equilibrium orbits. The transport system consists of four bending magnets (BM1, BM2, BM3 and BM4), three magnetic inflection channels (MIC1, MIC2 and MIC3), and an electrostatic inflection channel (EIC). The MICs are inserted in the gap between the pair of poles of the sector magnets to increase the bending power of the sector field locally. The EIC is placed in the position where the trajectories of injected beams match finally with the first equilibrium orbits. The radial-injection method as shown in Figure 1 is the most straightforward one adopted in many ring cyclotrons.

However, to apply the method on the SRC is more difficult than on a normal conducting ring cyclotron, because a strong negative fringe field exists in the valley and central region of the SRC and so the beam trajectory strongly depends on the acceleration condition.

	Charge	$E_{inj}$ (MeV/u)	$E_{ext}$ (MeV/u)
$^{16}\text{O}$	8+	127	400
$^{84}\text{Kr}$	30+	103	300
$^{238}\text{U}$	59+	58	150

Table 1: Energies of the injected and extracted beams in the full-power operation of the SRC.

In order to accept the changes in the beam trajectory, the elements should be movable or have a large bore.

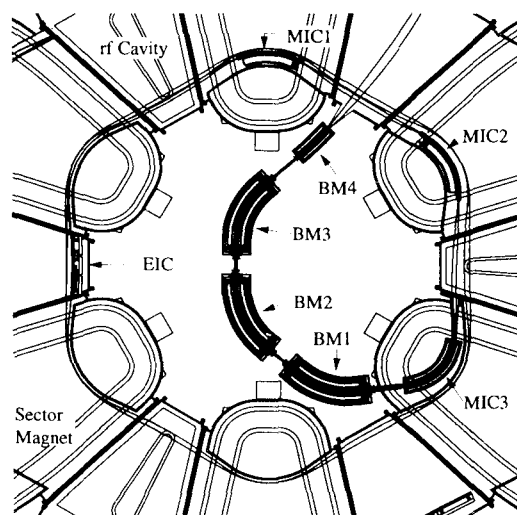


Figure 1: A schematic layout of injection elements for the SRC, and possible trajectories for the injected beam.

We have adopted the latter method for the elements, except for the EIC, which is required to move as large as 10 cm at the maximum in the radial direction. It is important to make the change of the beam trajectories inside the elements as small as possible. In the numerical analysis of the injection orbits[3], we concentrated our effort on minimizing them ( $\Delta x$ ). Results obtained from such an analysis are shown in Table 2, together with their parameters.

The four BMs (BM1-4) and MIC3 are required to be superconducting magnets in order to produce the required magnetic fields. In the following section, a design study of BM1 and MIC3 which are the most difficult to construct in the superconducting elements are described.

## 2 BM1

Specifications of the BM1 are listed in Table 3. There are three difficulties in the design of BM1. Firstly, we can not use an iron yoke for magnetic shielding because

	Radius (cm)	Angle (deg.)	B or E (max.) (T) or (kV/cm)	$\Delta x$ (cm)
EIC	—	—	110	7.0
MIC1	111	46.5	0.17	1.0
MIC2	110	52.5	0.28	1.0
MIC3	87	73.9	1.7	1.0
BM1	132	52.0	4.00	1.0
BM2	130.5	52.0	3.99	1.0
BM3	128	52.0	3.97	1.0
BM4	492.5	7.0	-0.67,+0.69	2.0

Table 2: Parameters of the injection elements and changes ( $\Delta x$ ) in the trajectories obtained from the numerical analysis of injection orbits.

Item	Value
Type	Iron free Active shield
Maximum field	4.02T
Homogeneity	$1 \times 10^{-3}$
Beam Bore	40 (Horizontal) $\times$ 20 (Vertical) mm <sup>2</sup>
Radius	1320mm
Angle	40deg.
Fringe Field	<100gauss
Space limit in the radial direction	about $\pm 20$ cm
Space for the coil end region	about 10cm

Table 3: Main specifications of the BM1.

the total flux of the stray field in the central region of the SRC is large enough to saturate the iron. We adopted active-shield-type magnets for the BMs although more magnetic motive force is needed than the case of an iron-shield-type magnet. Secondly, the space available for the BM1 is very limited; the BM1 has a space of as small as about 20 cm in the radial direction. In the coil-end region coil supports and cryostat walls need to be accommodated within the space of about 10 cm. Thirdly, the BM1 needs to consist of coils with negative curvature which are difficult to wind because cables can not be wound with tensions. Taking account of these three difficulties, we took cares of the following two points in the design of the BM1. Firstly, the coil structures should be simple. Secondly, it should be as effective as possible to generate the field, namely the spaces for the coils should be as small as possible in the radial and azimuthal directions. The new coil structure of the active-shield-type has been proposed to fulfill the two demands.

Figure 2 shows the proposed cross section and 3D-view of the coil structure. Eight current sheets located near the beam axis generate the magnetic field in the beam bore and the other four current sheets generate

the field to cancel the fringe field from the eight current sheets. Such configurations of the current sheets can realize the structure of coils that need not be bent up at the ends of the channel.

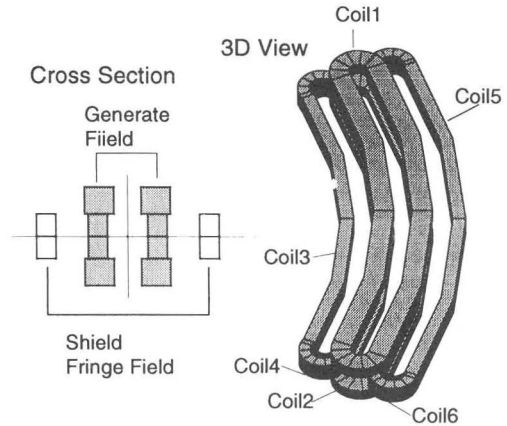


Figure 2: Coil structure of the BM1.

## 2.1 Magnetic Field

Two-dimensional analysis was carried out using OPERA-2D to optimize the coil sizes and locations[4]. Figure 3 shows a coil geometry and performance which can realize the specifications of the BM1. The magnetic field and Lorentz forces in the conductor region were also calculated. Figure 4 shows magnetic field in the coil when there is a stray field of 0.6T from the sector magnet of the SRC. The maximum field reaches up to about 5T at the left boundary of the coil1-2 and coil3-6 which needs to be supported carefully.

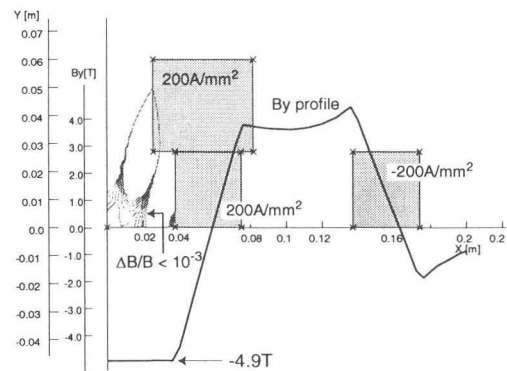


Figure 3: Field distribution and coil geometry of the BM1. Region where  $\Delta B / B$  is less than  $10^{-3}$  is indicated by contours.

Three-dimensional field analysis was carried out using OPERA-3D to study the coil end. Figure 5 shows the maximum field at the end of coil3-6. The coil end divided into the two sections was adopted to reduce the maxi-

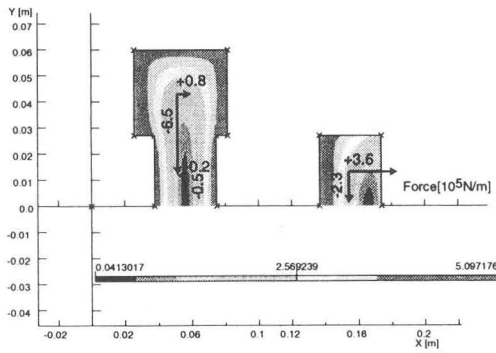


Figure 4: Strength of magnetic field in the coil region and moving forces on the coil when 0.6T stray field from the sector magnets exists.

imum magnetic field in this region by 1T. This makes the coil end stable against quench.

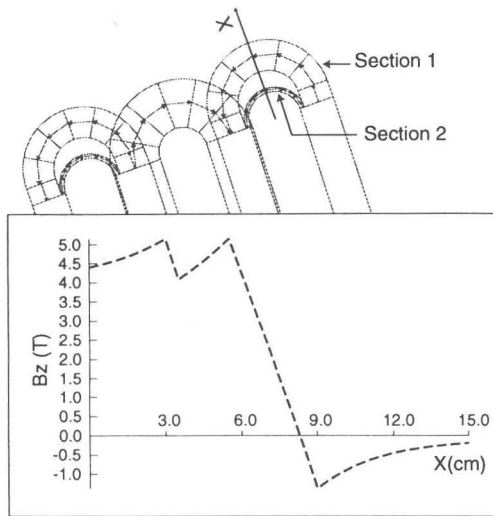


Figure 5: Geometry and the maximum field of the coil end.

## 2.2 Support Structure

Figure 6 shows the cross section of the coil support structure. The coils are mainly supported in the horizontal and vertical direction by a pair of continuous clamps and bolts, respectively. The pre-stress required to keep the coil in compression when the magnet is excited is provided by Cotta, Bolt1 and Bolt2 in Figure 6. Each required pre-stress was estimated by taking account of the shrink and deformation of the coils and the support materials in assembling, cool-down and excitation.

When the magnet is cooled down, the support structures and the coils shrink with different rates. The differences of the relative shrink rates of the coil  $\alpha$  to the support structures are listed in the Table 4. The negative value means that the stress in the coil decrease. In the excitation, Lorentz forces shrink the coils and deform the

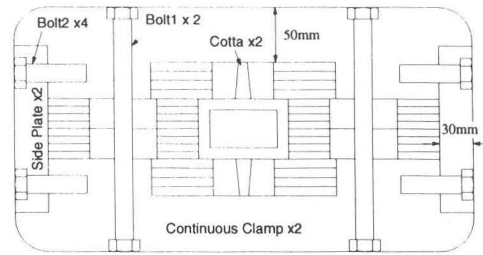


Figure 6: Cross section of the coil support structure.

support structures. These deformations have the effects to decrease the stress in the coil. The shrink of the coils and the deformations were calculated using OPERA-2D, as shown in Figure 7. Total pre-stress required in the assemble can be calculated according  $\sigma_1 = E \times (\alpha + \beta - \gamma)$  where  $E$ ,  $\beta$  and  $\gamma$  represent the elastic modulus of the coil assumed to be 20 MPa, the ratios of the shrink of the coil and the deformation of the support relative to the coil size respectively. The maximum stresses of the coil shown in Table 4 are less than the their typical values of the yield strengths which are 70MPa for the insulation of the coil. Further analysis and optimization of the support structure can decrease the maximum stress of the coil3-6.

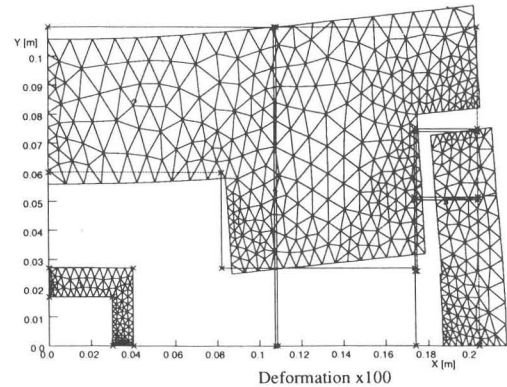


Figure 7: Deformation of the coil supports due to electromagnetic forces.

	$\alpha$ [ $10^{-3}$ ]	$\beta$ [ $10^{-3}$ ]	$\gamma$ [ $10^{-3}$ ]	$\sigma_1$ [MPa]	$\sigma_2$ [MPa]
Coil1-2					
H	-0.75	-0.34	0.84	-38.6	-14.9
V	-1.50	-0.25	0.58	-16.6	-13.0
Coil3-6					
H	-0.25	-0.36	1.73	-46.8	-15.8
V	-1.50	-0.00	1.84	-66.8	-7.0

Table 4: Summary of structural analysis on the cross section of the support structure. See the definition of  $\alpha$ ,  $\beta$ ,  $\gamma$  and  $\sigma_1$  in the text.  $\sigma_2$  represents the maximum stress in the coil region in the case of excitation.

The support of the coil end is the most important to prevent the coil quench. The 3D magnetic analysis of the magnetic fields and Lorentz forces discussed in section 2.1 shows that the inside boundaries of the coil ends are easy to quench. The support material (high Mn steel) inside of the each coil can support that boundary well because the high Mn steel shrink less than the coil and push the coil end after cool-down.

### 2.3 Helium Vessel and Cryostat

Figure 8 shows the cross section of the whole structure. All the coils and the support structures are installed in a He vessel of about 7mm in thickness for the outer chamber and 10mm for the inner chamber. The inner chamber is also used for the support structure. If necessary, helium channels can be made in the coil supports.

All the 4.5 K materials are installed in a cryostat and suspended with support links. A water-cooled beam pipe which is surrounded by an 80 K shield is installed in the center of the BM1 to form warm-bore. Mechanical design of the cryostat is in progress.

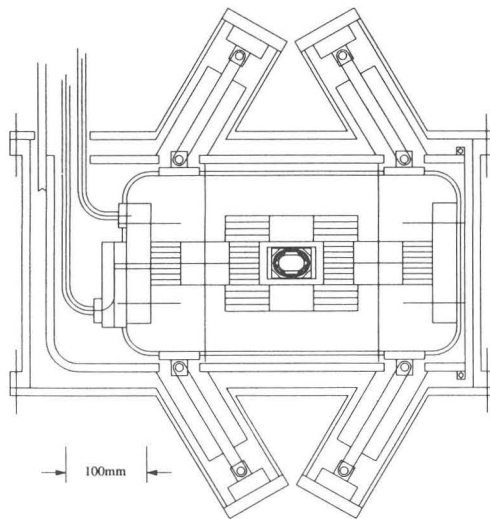


Figure 8: Cross section of the BM1 including a cryostat.

### 3 for Installation of 4 Cavities

The injection and extraction systems studied so far are designed for a three-cavity configuration. Now we are studying the systems which allows us to install four cavities in the SRC, in order to have larger orbit separation for better beam extraction. Figure 9 shows a preliminary drawing of the SRC with four cavities and a flattop cavity. Some of the injection and extraction elements in the case of four cavities are more difficult than those in

the case of three cavities. After the conceptual design of them we will compare the two systems.

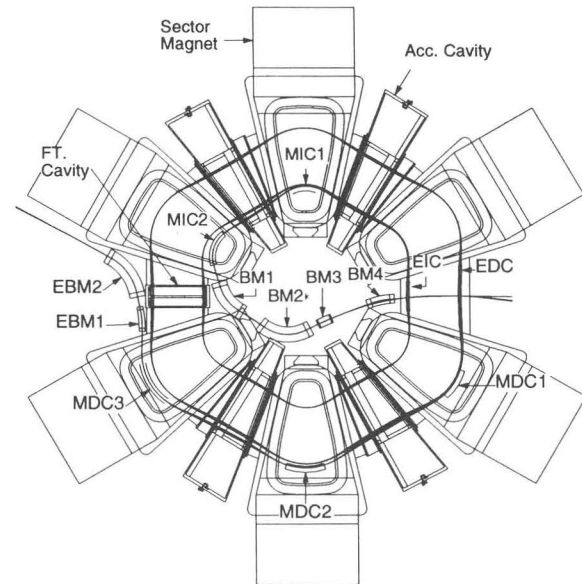


Figure 9: Preliminary drawing of the injection and extraction systems of the SRC with four cavities and a flattop cavity.

### References

- [1] Y. Yano et al.:in this proceedings.
- [2] A. Goto et al.:in this proceedings.
- [3] S. Fujishima et al.:in this proceedings.
- [4] T. Tominaka et al.:in this proceedings.